Int J Adv Manuf Technol (2016) 86:1319–1328
DOI 10.1007/s00170-015-8260-2

ORIGINAL ARTICLE

Fabrication of nanopillar arrays by combining electroforming and injection molding

Bing-yan Jiang[1,2] · **Ming-yong Zhou**[1,2] · **Can Weng**[1,2] · **Lu Zhang**[1,2] · **Hui Lv**[1,2]

Received: 6 September 2015 / Accepted: 17 December 2015 / Published online: 9 January 2016

Abstract Injection molding is regarded as one of the cost-effective molding technologies to produce polymer items in large numbers. In this paper, a fabrication method for nanopillar arrays by combining electroforming and injection molding has been proposed. Mold inserts with satisfactory replication and high homogeneity have been electroformed by a self-designed micro-electroforming equipment. A variotherm injection molding technique with electrical heating and oil cooling has been realized for precise temperature control on mold cavity. It is shown that the mold cavity temperature can be represented by the measured temperature of the thermocouple installed in the mold. Nanopillars are found to be almost filled during the packing stage. Circular structures at the top of nanopillars have been observed under a lower packing pressure. As a key processing parameter, mold temperature is recommended as 25 °C higher than the polymer glass transition temperature. To ensure better replication quality of nano-patterns, the demolding temperature should be around 10 °C lower than the polymer glass transition temperature.

Keywords Nanopillar array · Electroforming · Injection molding · Processing parameter

✉ Can Weng
canweng@csu.edu.cn

[1] College of Mechanical and Electrical Engineering, Central South University, Changsha, Hunan 410083, People's Republic of China

[2] State Key Laboratory of High Performance Complex Manufacturing, Central South University, Changsha, Hunan 410083, People's Republic of China

1 Introduction

Polymer products with nanostructures have excellent mechanical and optical properties, chemical resistance, and other advantages over more commonly nanostructured materials [1–3]. Injection molding is regarded as one of the cost-effective technologies to produce polymer items in large numbers. Sub-micrometer/nanometer surface structures have been successfully fabricated by injection molding in recent years [4, 5]. Compared to traditional injection molding, the filling quality of nanostructures is very sensitive to process variations [6–11]. Nanostructures have been found to be filled mainly in the packing stage [12]. A durable master with well-fabricated nano-scale features is a fundamental component of an injection mold for mass production. Researchers firstly wrote nanostructure patterns on silicon plates by electron beam lithography (EBL) and then embedded them in the mold for injection directly. Due to the huge difference of thermal expansion coefficient between silicon and polymeric materials, the silicon plate can be broken easily, thus having a limited working life [13]. Hybrid polymeric inlays, patterned by nano-imprint lithography, were used to rapidly mass replicate pillar-like nanostructures by injection molding [14]. However, the replicated nanostructures were stretched up to 40 % of their designed height. Because of superior mechanical properties and durability of metal materials, metal masters, such as nickel stamps, have been widely used as micro/nano-molds [15]. Nano-patterns from silicon plates could be transferred to the metal masters effectively by electroforming process and other methods.

The main purpose of this paper is to propose a feasible fabrication method for nanopillar arrays by combining electroforming and injection molding. Electroforming equipment with a moveable cathode is self-designed. Nickel mold inserts with high homogeneity are fabricated by adjusting the

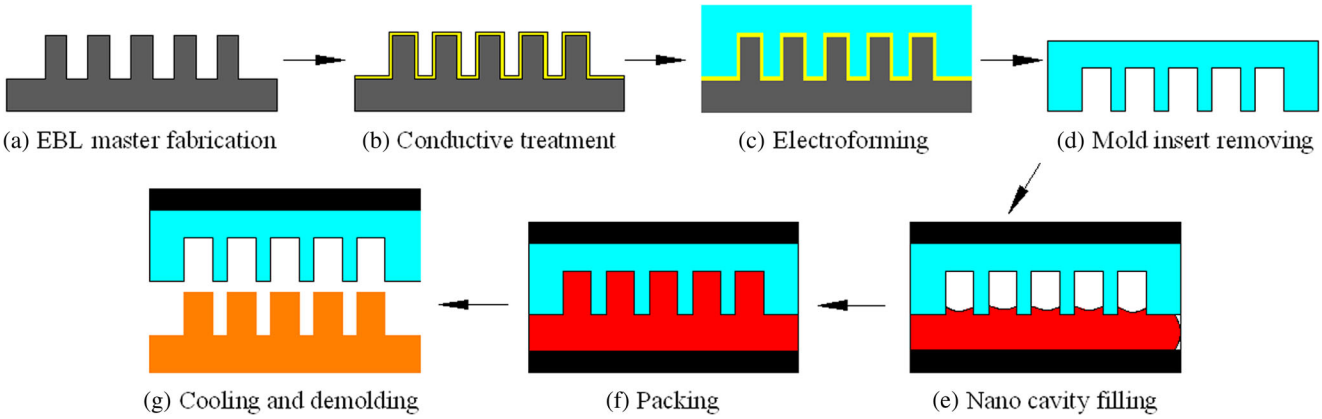

Fig. 1 Outline of the steps involved in producing nanopillar arrays: master structures made of silicon (**a**) are patterned by electron beam lithography. The master is conductive treated by high vacuum sputtering (**b**) before electroform deposition (**c**). The separated nickel mold insert (**d**) is employed in the filling (**e**), packing (**f**), cooling, and ejection (**g**) phases during the injection molding process

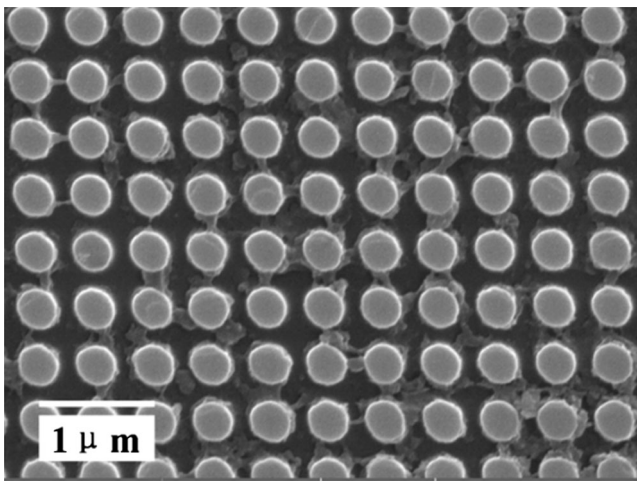

Fig. 2 SEM image of silicon master with nanopillars fabricated by electron beam lithography. The pillars of width $w = 380nm$ and height $h = 300nm$ are located on a square grid of pitch p = 500nm

moving parameters. The injection mold with a variotherm molding technique with precise temperature control is constructed. Effects of the main injection molding processing parameters on the average heights of molded PMMA nanopillars are investigated. The flowing and filling behaviors of the polymer melt in the nano-cavities are further identified.

2 Injection mold and mold inserts

A summary of the process steps involved in producing nanopillar arrays is presented in Fig. 1. Arrays of 380-nm wide and 300-nm high pillars in a square grid of pitch 500 nm, as shown in Fig. 2, were fabricated on silicon by EBL (Raith 150, Raith® Corp., Germany). The patterned areas were $200 \times 200\ \mu m^2$ in size.

2.1 Mold inserts with nanostructure fabrication

To meet the high replication requirements of electroformed mold inserts for micro- or even nano-structures, micro-electroforming equipment was self-designed with a moveable

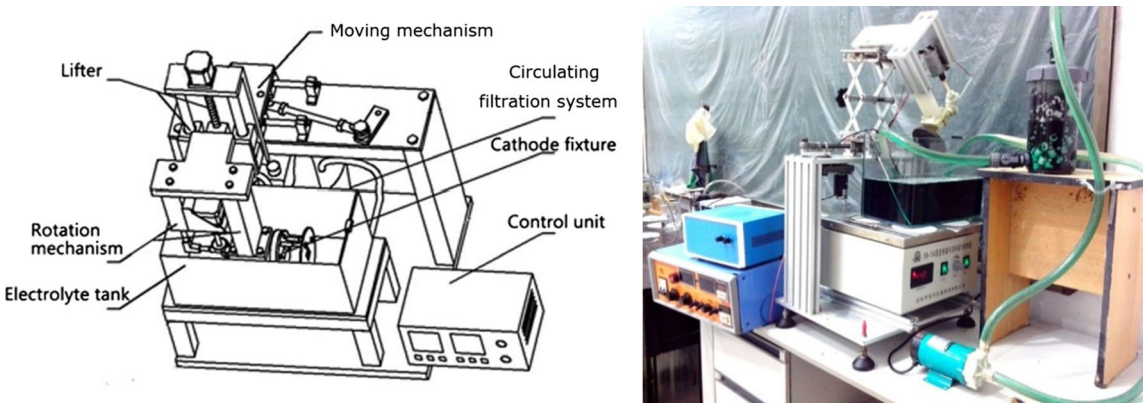

Fig. 3 Self-designed micro electroforming equipment with a movable cathode

Table 1 Major ingredients of electrolyte and their contents

Ingredient	Content
Nickel bis(sulphamidate)	450 g/L
Nickel chloride	15 g/L
Boric acid	30 g/L
Sodium 2-ethylhexyl sulfate	4 ml/L
Saccharin sodium	0.2 g/L

mainly retained in the anode. The master was then successively cleaned in an ultrasonic cleaner by ethanol and distilled water before electroforming.

The major ingredients of electrolyte and their contents are listed in Table 1. During the electroforming process, the electrolyte was kept at the pH value of 3.5~4.5 and the temperature of 45~50°C. Rectangular pulse current, with frequency of 1500 Hz and duty ratio of 24 %, was used in this experiment. The average current density was about 4 A/dm^2, while the initial current density was 1 A/dm^2 to avoid coarse grains. The anode was an electrolytic nickel plate with the size of 65 mm × 55 mm × 4 mm, and the initial distance between the

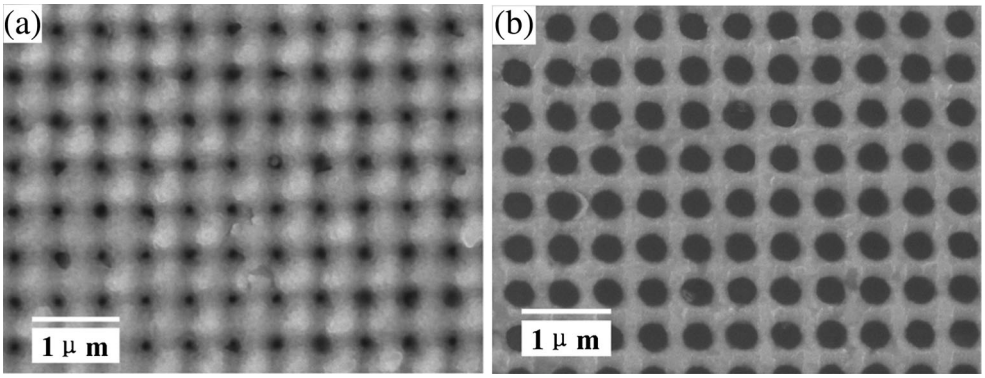

Fig. 4 SEM images of nanostructures on the nickel-electroformed mold inserts with a fixed cathode (**a**) and with a movable cathode (**b**)

cathode regarding the enhancement of mass transfer. This equipment includes a control unit, a cathode movement system, and an electrolyte circulating filtration system. The schematic diagram and photo of micro-electroforming equipment are presented in Fig. 3. A 20-nm thick Au film was coated on the silicon master carrying nano-patterns for conductive treatment by a high vacuum sputter coater (EMSCD500, Leica® Corp., Germany). In order to ensure the qualities of nano-patterns during the lift-off process, a passivation treatment was performed using a solution of potassium dichromate and water. Because of the passivation treatment, the Au layer was anode and the cathode was 100 mm. Two nickel mold inserts were electroformed with a fixed cathode and a movable cathode, respectively. With a movable cathode, the rotation speed was 150 r/min and the reciprocation speed was 250 mm/min. Fig. 4 compares the nanostructures, measured by FESEM (Mira 3, Tescan® corp., Czech Republic), on the two electroformed nickel mold inserts with a fixed cathode and a movable cathode. It was found that the replication quality of the electroformed mold insert was significantly improved with a movable cathode. This is due to that the movement of cathode can promote

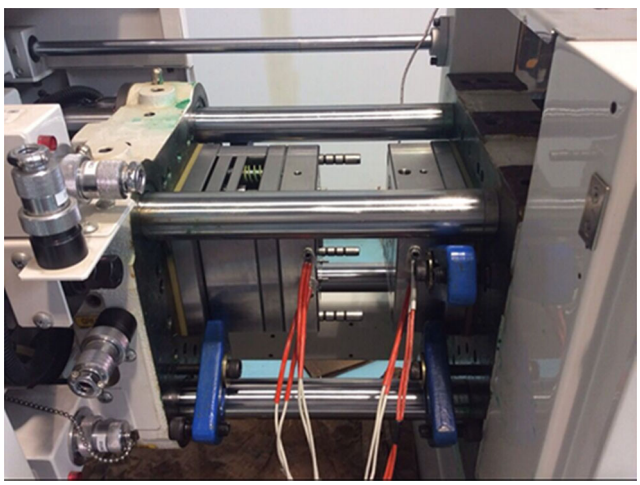

Fig. 5 Injection mold for nanopillar arrays

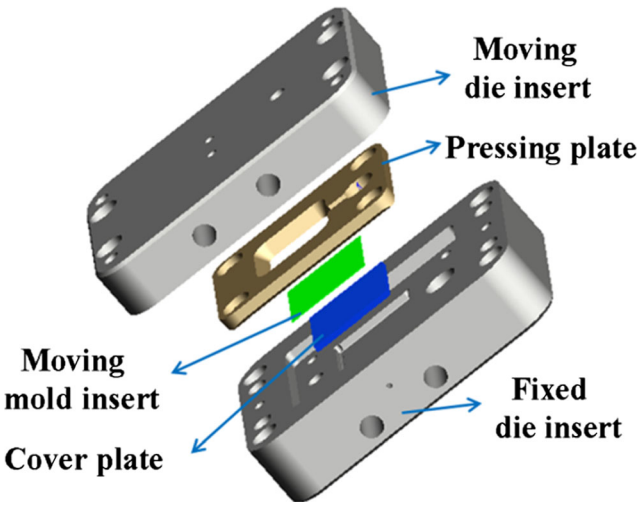

Fig. 6 Schematic diagram of the mounting structure for the mold inserts

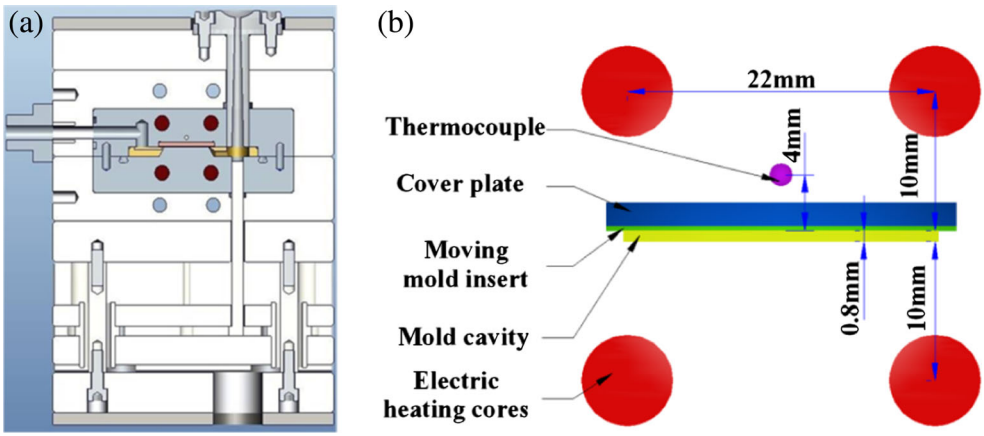

Fig. 7 Installation diagram of four electrical heating rods and a thermocouple

the flow of electrolyte near the electrode surfaces, thus increasing the mass transfer rate around the nanostructures. With the help of cathode movement, a mold insert with around 400-μm thick nickel layer was fabricated after 24 h non-stop electroforming. To avoid the influence of thickness non-uniformity during the electroforming process, the mold insert was polished to 300 μm. The mold insert carrying nanostructures was a 25 mm × 25 mm rectangle. The diameters of nano-cavities were measured by SEM and its analysis software (Image-Pro Plus). The average value of diameters was measured at 344 ± 10 nm, and the depth was about 297 ± 12 nm. The decreased diameters of nano-cavities were mainly due to the existence of internal stresses during the electroforming process. The electroformed mold insert was further visualized and measured by an atomic force microscope (Dimension Icon, Bruker® corp., Germany). The electroformed mold insert with high homogeneity and replication precision could be applied to the following injection molding process.

2.2 Injection mold

The injection mold (presented in Fig. 5) was designed to be capable of air pumping and variotherm molding. The moving mold insert, carrying nanostructures, was electroformed by self-designed micro-electroforming equipment mentioned above. A pressing plate and a cover plate, as shown in Fig. 6, were added between the die inserts of moving and fixed halves to protect the easily deformed moving mold insert from the high forces generated during the molding process.

A variotherm injection molding technique with electrical heating and oil cooling was realized in this mold. Four electrical heating rods were symmetrically arranged around the mold cavity, as shown in Fig. 7. The mold cavity was surrounded by the moving mold insert, the pressing plate, and the moving die insert. The cavity length was 20 mm, the width was 20 mm, and the depth was 0.8 mm. A thermocouple (TJ36, Omega® Corp., USA) was located 4 mm above the moving mold insert on the fixed part side to acquire the temperature there. For the heat dissipation from the mold surfaces, the mold cavity temperature is different from the set temperature by a mold temperature controller of the injection molding machine. As a key processing parameter, the mold cavity temperature is analyzed in the coming section.

3 Characterization of mold cavity temperature

For products with micro- or nano-structures, the mold cavity temperature is particularly important for replication quality and dimensional precision. The mold cavity temperature could be approximately measured by the thermocouple in the designed mold, but there is a slight difference due to the 4-mm distance from the thermocouple to the mold surface.

Table 2 Thermo-physical properties of mold materials

Component	Material	Thermal conductivity	Density $\rho(g/cm^3)$	Specific heat $c_p(J/(g \cdot K))$
Cover plate	Heat-resistant epoxy resin	0.59	1.80	1.60
Fixed and movable mold plates	GS-2316 die steel	24.3	7.75	0.46
Other mold bases	1.7311 structural steel	49.8	7.85	0.49
Mold inserts	NAK80 die steel	41.3	7.72	0.46
Electrical bar	304 stainless steel	16.2	7.93	0.50

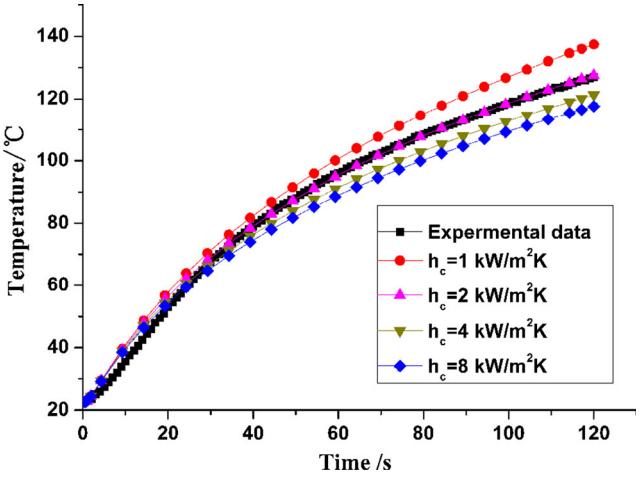

Fig. 8 Changes of mold temperatures with heating time from simulations and experiments

3.1 3D numerical simulation

The 3D simulation model based on the ANSYS® commercial software is established. The model is meshed with a tetrahedral mesh method. The mold inserts are supposed to have an excellent contact with the mold base. The thermal conductivities between them are set to be a constant. The ambient temperature is set to 22.5 °C. The mold materials are set to be homogeneous. Table 2 lists the thermo-physical properties of mold materials which are used in the simulations.

The initial mold temperature is the same as the ambient temperature (22.5 °C). The heating time is set to 120 s in simulations. In the mold heating process, the interfacial thermal contact resistance between mold inserts and mold plates would significantly influence the mold temperature distribution. The value of interfacial thermal contact resistance cannot be measured directly, determined by multi-factors, such as material properties, contact surface temperature, contact pressure, and surface roughness. By comparing the mold cavity temperatures from simulations and experiments, the interfacial thermal conductivity can be estimated. Interfacial thermal conductivity is the reciprocal of thermal contact resistance. In simulations, the interfacial thermal conductivity is set to: $1kW/(m^2 \cdot K)$, $2kW/(m^2 \cdot K)$, $4kW/(m^2 \cdot K)$ *and* $8kW/(m^2 \cdot K)$, respectively.

3.2 Experimental verification

The changes of mold temperatures with heating time from both simulations and experiments are demonstrated in Fig. 8. When the interfacial thermal conductivity between mold inserts and mold plates was $2kW/(m^2 \cdot k)$, the simulation results agreed well with experimental results. The mold cavity temperature near the thermocouple increased from 22.5 to 127.5 °C in 120 s, with a decreasing heating rate.

The mold cavity is encircled by the moving mold insert, the moving die insert, and the coving plate. The upper surface of mold cavity is in the moving die insert, marked out with a white dotted rectangle in Fig. 9a. With a confirmed interfacial thermal conductivity of $2kW/(m^2 \cdot K)$, the temperature distribution of moving die inserts after 120 s of heating is demonstrated in Fig. 9a. The average temperature of the upper surface was 127.7 °C from the simulation. The temperature difference in this area was less than 4 °C. The lower surface of mold cavity is in the moving mold insert, also marked out with a white dotted rectangle in Fig. 9b. The average temperature of the lower surface was 123.3 °C, with around 3.9 °C temperature difference in this area. From the simulation, the average temperature of mold cavity surfaces was 125.5 °C, about 2 °C lower than the measured temperature by the thermocouple. As the temperature difference was acceptable, the mold cavity temperature could be represented by the measured temperature of the thermocouple.

Figure 10 demonstrates mold temperatures captured by the thermocouple in electrical and oil heating with a set mold temperature of 110 °C in two mold cycles, respectively. It seems that the electrical heating could obviously improve the heating efficiency and the temperature control accuracy. The cooling rates of the two curves were comparable due to the same oil cooling method adopted. The mold temperature fluctuated between 85 and 93 °C by oil heating. Since the mold temperature cannot be accurately controlled, oil heating is not suitable for nano- or micro-injection molding.

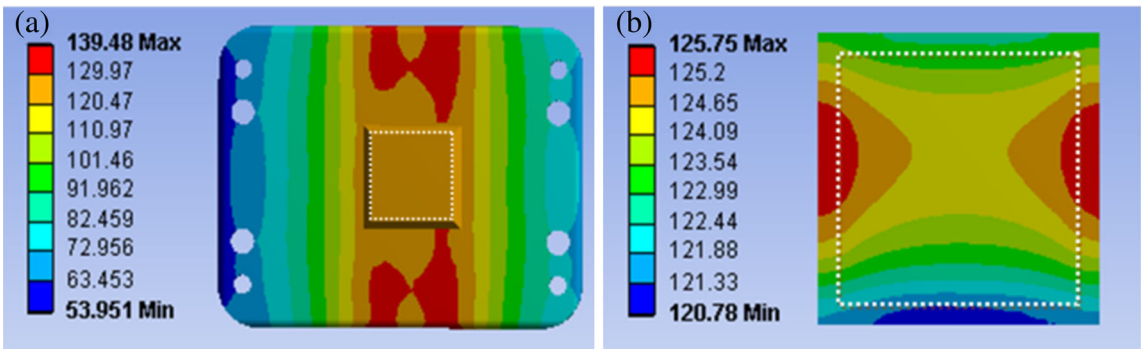

Fig 9 Temperature distributions of mold cavity surfaces in the simulation. **a** moving die insert; **b** moving mold insert

4 Injection molding of nanopillar arrays

Injection molding was conducted with polymethyl methacrylate (PMMA, Mitsubishi® Acrypet TF-8) in a Sodick® LD05EH2 injection molding machine (max injection pressure 197 MPa, plunger diameter 12 mm). Mold temperature, melt temperature, packing pressure, packing time, and cooling time are investigated to study their effects on the replication quality of nanostructures, characterized by the average height of polymeric nanopillars. An atomic force microscope (Dimension Icon, Bruker® corp., Germany) was used to measure the heights of nanostructures. Fifteen or more nanopillars near the center of the molding parts were measured to obtain the average heights under each molding condition. Table 3 lists the processing parameters used in this study. At least five levels of each parameter were tested. It is reported that the mold temperature and the packing pressure are two main parameters affecting the quality of molded nano-structures [8, 10]. The numbers of the two parameters were thus increased to six. The values of the packing time used in initial experiments were 0, 1, 3, 5, 7, and 9 s, respectively. It was found that the average heights of nanopillars varied greatly when the packing time was increased from 0 to 1 s. Three reference points of the packing time were then added between 0 and 1 s.

5 Results and discussion

The molded part with its runner system is shown in Fig. 11. Mold temperature was obtained by the thermocouple installed in the mold as mentioned in Section 2.2. Effect of the mold temperature on the average heights of PMMA nano-structures is presented in Fig. 12a.

The values of average height for PMMA nanostructures present an increasing trend with the increase of mold temperature. With a lower mold temperature, the substrate was well replicated while nanostructures were poorly replicated, due to the rapid solidification of the melt contacting the mold surfaces. With the increase of mold temperature, the solidification rate of the skin melt decreases; thus, the replication heights of nanostructures increase. When the mold temperature was higher than the PMMA glass transition temperature ($T_g = 101\,^{\circ}\mathrm{C}$), the polymer melt was easily filling into nanostructures. It seems that well-replicated nanopillars can be obtained with the mold temperature about 25 °C higher than the polymer glass transition temperature. In micro-injection molding, the mold temperature is recommended to be around the polymer glass transition temperature for better replication [6, 7].

High-quality replication requires both complete filling of the mold structures by the polymer melt and, equally important, negligible deformation of the solidified replica during demolding. With a higher mold temperature ($\geq 130\,^{\circ}\mathrm{C}$), nano-patterns would be fully filled. When the mold temperature was 150 °C, the measured average height of molded nanopillars was 306 ± 43 nm. The value was obviously larger than the average depth of the nano-cavities on the electroformed mold insert. Some of the nanopillars even reached a height of 340 nm. Under a higher mold temperature, the interface adsorption

Table 3 Processing parameters used in this study

Processing conditions	Values
Mold temperature (°C)	50, 70, 90, 110, 130, 150
Melt temperature (°C)	210, 225, 240, 255, 270
Packing pressure (MPa)	20, 40, 60, 80, 100, 120
Packing time (s)	0.25, 0.5, 0.75, 1, 3, 5, 7, 9
Cooling time (s)	10, 20, 30, 40,50

Bold-faced type means the default standard conditions. The standard conditions were used while other values were varied.

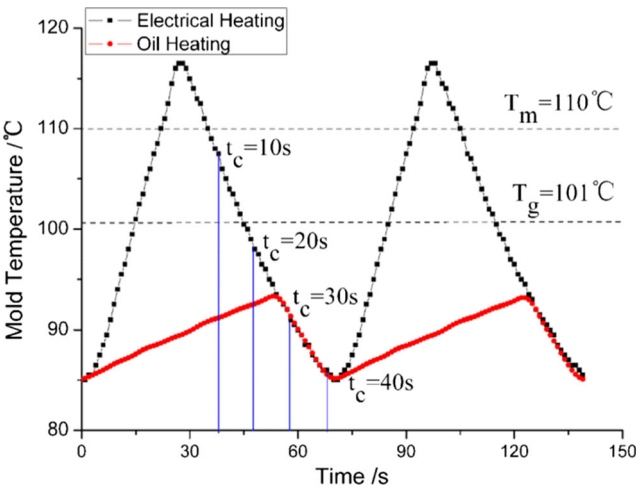

Fig. 10 Mold temperatures in two molding cycles captured by the thermocouple in electrical or oil heating and oil cooling with a set mold temperature of 110 °C

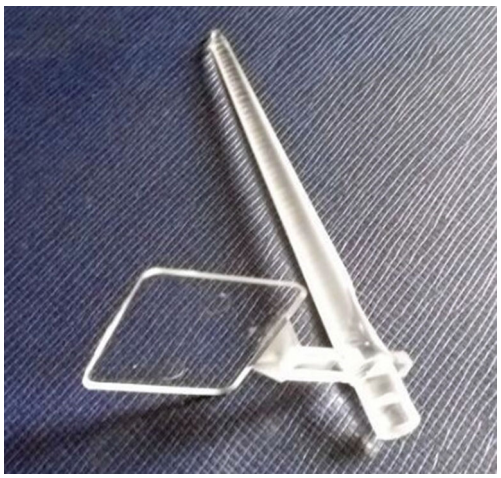

Fig. 11 PMMA injection-molded nanopillar array with its runner system

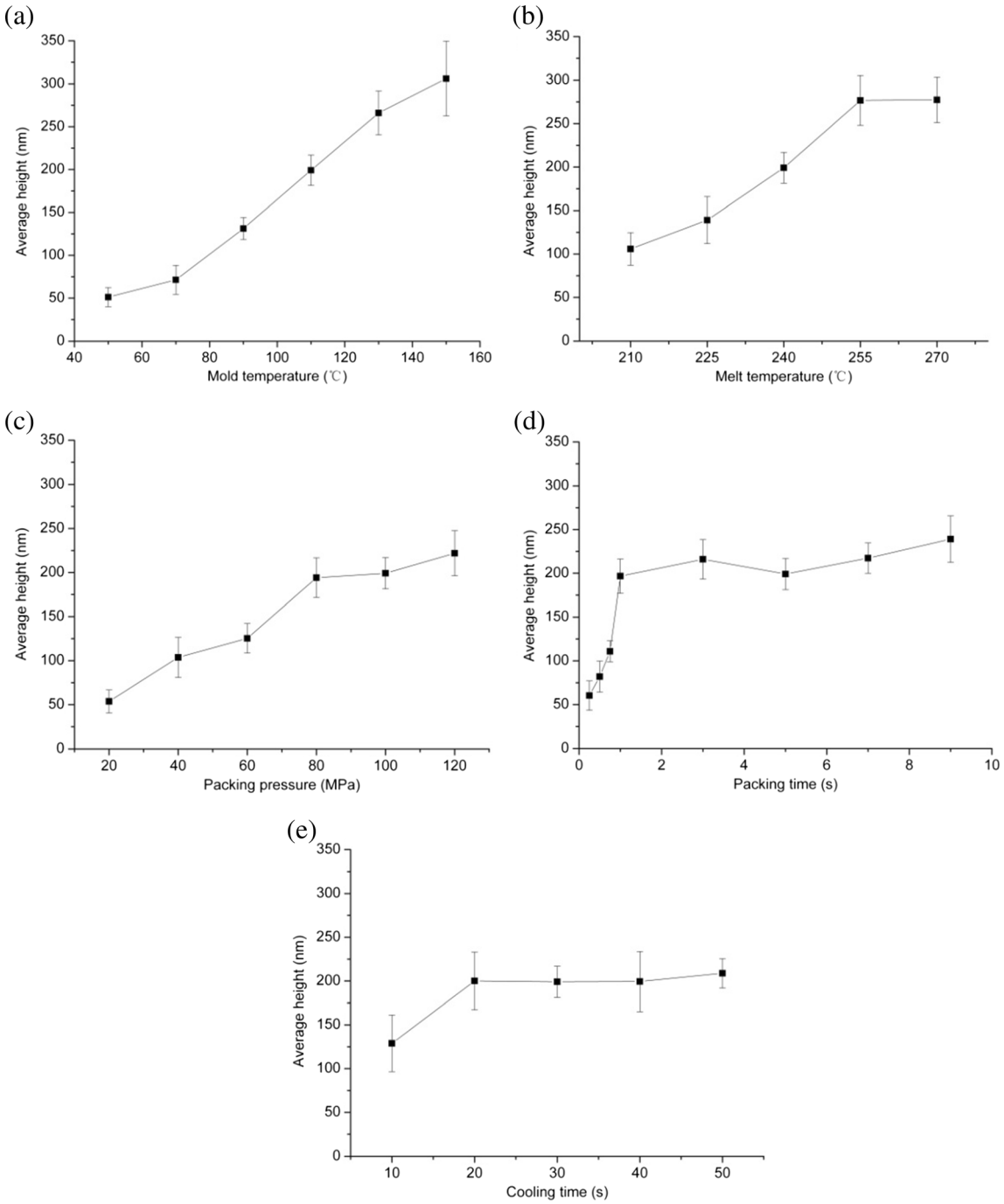

Fig. 12 Effects of processing parameters on the average heights of PMMA nanostructures. **a** Mold temperature, **b** melt temperature, **c** packing pressure, **d** packing time, and e cooling time

force increased with the increasing contact area between the polymer melt and the mold nanostructures. With the same cooling time (30 s), a higher mold temperature brought a higher demolding temperature, at which the polymer possessed a lower tensile strength. During the demolding process, nanopillars with a lower tensile strength would be stretched to some extent, bringing a larger height. Nevertheless, some nanopillars would be fractured during demolding (as shown in Fig. 13).

Mold temperatures in two injection molding cycles were captured by the thermocouple with a set mold temperature of 110 °C, as demonstrated in Fig. 10. The temperature curve was steady in every cycle time (around 70 s). Maximum mold temperature was recorded as 117 °C, slightly higher than the set temperature. Different cooling times correspond to different demolding temperatures. When the cooling time was 10s ($t_c = 10s$), the demolding temperature ($T_d = 107°C$) was still higher than the PMMA glass transition temperature.

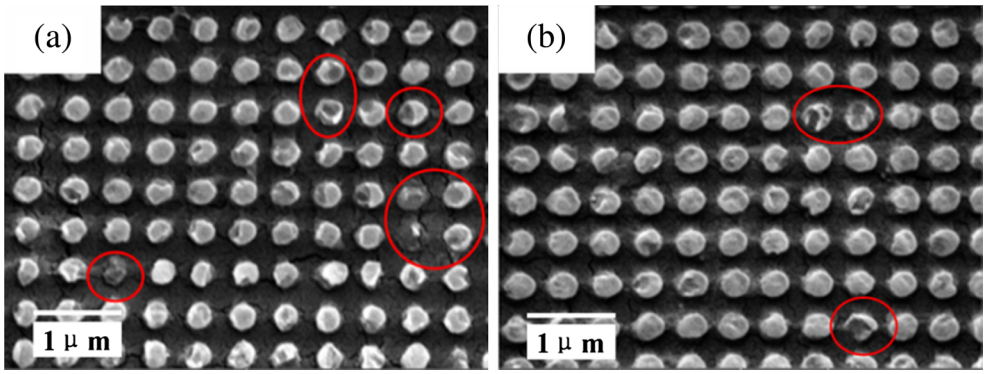

Fig. 13 SEM images of replicated PMMA nanopillar arrays with some fractured nanopillars during demolding. **a** Mold temperature was 150 °C. **b** Mold temperature was 130 °C

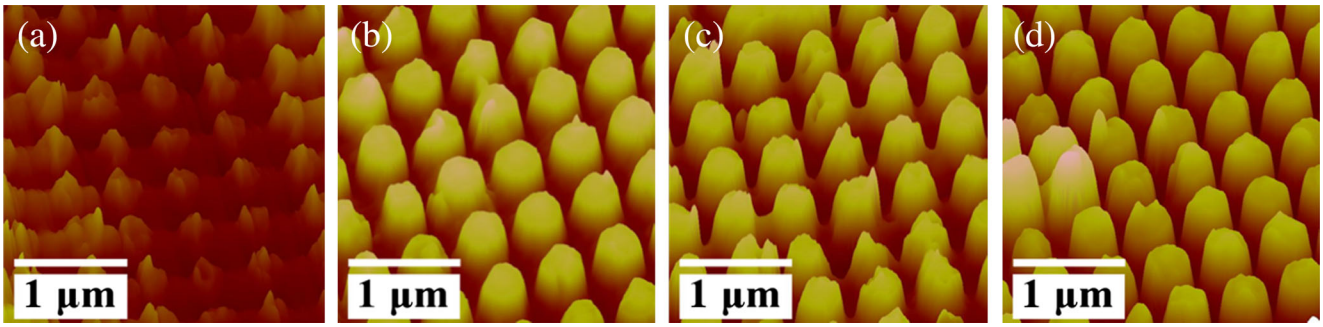

Fig. 14 AFM images of replicated PMMA nanopillar arrays with different cooling times . **a** $t_c = 10s$, $T_d = 107°C$, **b** $t_c = 20s$, $T_d = 98°C$, **c** $t_c = 30s$, $T_d = 90°C$, and **d** $t_c = 40s$, $T_d = 85°C$

Nanostructures at that demolding temperature were badly damaged during demolding, as presented in Fig. 14a. When the cooling time was larger than 20 s (as shown in Fig. 14b–d), PMMA nanopatterns were well formed after ejection with a lower demolding temperature. Figure 12e shows the effect of the cooling time on the average heights of PMMA nanopillars. The average heights rapidly increased when the cooling time was increased from 10 to 20 s and then slightly varied from 20 to 50 s. To ensure the better replication quality of nanostructures, it seems that the demolding temperature should be around 10 °C lower than the polymer glass transition temperature.

Effect of the melt temperature on the replicated average heights of PMMA nanopillars is shown in Fig. 12b. With the increase of melt temperature, the average heights of

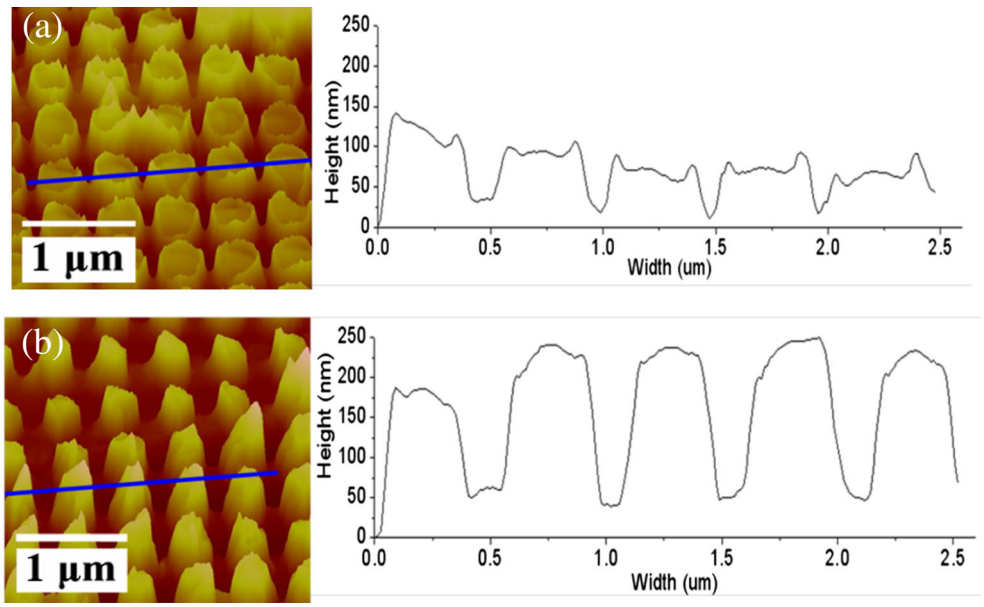

Fig. 15 AFM images of replicated PMMA nanopillar arrays under different packing pressures. **a** $P = 40MPa$ and **b** $P = 120MPa$

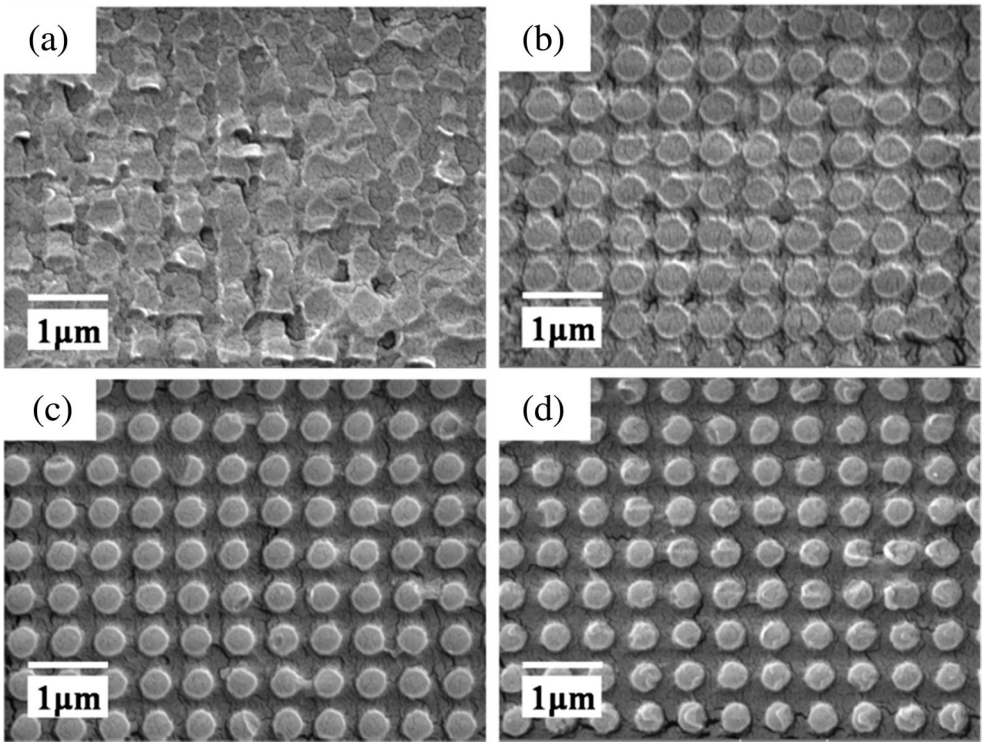

Fig. 16 SEM images of molded PMMA nanopillar arrays with different packing times. **a** $t_p = 0s$, **b** $t_p = 0.25s$, **c** $t_p = 1s$, and **d** $t_p = 9s$

nanopillars were increased. Nevertheless, the increase was not so obvious compared to that of mold temperature. It is reported that the packing pressure plays an important role in the filling of the micro/nanostructures [10, 12]. Figure 12c presents the effect of the packing pressure on the average heights of PMMA nanopillars. Packing pressure supplied the main driving force for polymer melt filling into nanostructures. With the increase of the packing pressure, the average heights of PMMA nanopillars were remarkably increased. When the packing pressure was lower than 80 MPa, it was observed that there were circular structures at the top of nanopillars (as shown in Fig. 15a). Under a lower packing pressure, the interfacial tension between the melt and the mold promoted the filling of polymer melt into nanostructures. During the filling stage, a largest flow rate of melt occurred near the mold surfaces. With the increase of packing pressure, the circular structures were increasingly obscure (as shown in Fig. 15b). With a higher packing pressure, the packing pressure dominated the melt filling into nanostructures overwhelming the interfacial tension.

With the packing pressure of 100 MPa, effect of the packing time on the replicated nanostructures is investigated, as demonstrated in Fig. 12d. The value of average height was rapidly increased with the increase of packing time from 0 to 1 s and then slightly changed from 1 to 9 s. Nanopatterns were rarely filled during the filling stage, as shown in Fig. 16. It was found that the polymer melt seemed to fill the nanostructures during the packing stage, with similar results by Lin et al. [10].

6 Conclusions

In this paper, a fabrication method of nanopillar arrays has been presented by combining electroforming and injection molding techniques. Arrays of 380-nm wide and 300-nm high pillars in a square grid of pitch 500 nm were fabricated on silicon by EBL. Nickel mold inserts transferring nanostructures with 334 nm average width and 297 nm average depth were electroformed by a self-designed micro-electroforming equipment with a movable cathode. A variotherm injection molding technique with electrical heating and oil cooling was realized for accurate mold cavity temperature control. By comparing the mold cavity temperatures from simulations and experiments, the interfacial thermal conductivity was estimated as $2kW/(m^2 \cdot K)$. From the simulation, the average temperature of mold cavity surfaces was 125.5°C, about 2° C lower than the measured temperature by the thermocouple. As the temperature difference was acceptable, the mold cavity temperature could be represented by the measured temperature of the thermocouple. The PMMA nanopillar arrays were successfully injection-molded. Effects of the main processing parameters on the average heights of nanostructures were investigated. Mold temperature is one of the most important parameters. Well-replicated nanopillars could be obtained with the mold temperature about 25 °C higher than the polymer glass transition temperature. However, demolding temperature should be around 10 °C lower than the glass transition temperature. A higher mold temperature brought a higher demolding temperature, at which the polymer nanopillars

possessed a lower tensile strength. When the mold temperature was 150 °C, the molded nanopillars were indeed found to be stretched with the average height of 306 nm. Other parameters, such as the melt temperature and the packing pressure, also had influences on the replication heights of nanopillars. Nano-patterns were rarely filled during the filling stage. It was found that the polymer melt seemed to fill the nanostructures during the packing stage. Obvious circular structures at the top of nanopillars were observed under a lower packing pressure for the first time, caused by the interfacial tension between the melt and the mold. The mechanisms of molecular motions in nano-cavities during injection molding will become an important research field in our future work.

Acknowledgments The authors would like to acknowledge financial support from the National Natural Science Foundation of China under grant nos. 51305465 and 91123012. The authors also would like to express their sincere thanks for the technical support of silicon masters provided by the Institute of Physics of the Chinese Academy of Sciences.

References

1. Yang C, Yin XH, Cheng GM (2013) Microinjection molding of microsystem components: new aspects in improving performance. J Micromech Microeng 23:093001
2. Utko P, Persson F, Kristensen A, Larsen NB (2011) Injection molded nanofluidic chips: fabrication method and functional tests using single-molecule DNA experiments. Lab Chip 11:2303–2308
3. Chen H, Zhang Q, Chou SY (2015) Patterning of light-extraction nanostructures on sapphire substrates using nanoimprint and ICP etching with different masking materials. Nanotechnology 26: 085302
4. Macintyre D, Thoms S (1998) The fabrication of high resolution features by mould injection. Microelectron Eng 41(2):211–214
5. Schift H, David C, Gabriel M, Gobrecht J, Heyderman LJ, Kaiser W, Koppel S, Scandella L (2000) Nanoreplication in polymers using hot embossing and injection molding. Microelectron Eng 53(14):171–174
6. Liou AC, Chen RH (2006) Injection molding of polymer micro-and sub-micron structures with high-aspect ratios. Int J Adv Manuf Technol 28(11–12):1097–1103
7. Mönkkönen K, Hietala J, Pääkkönen P, Pääkkönen EJ, Kaikuranta T, Pakkanen TT, Jääskeläinen T (2002) Replication of submicron features using amorphous thermoplastics. Polym Eng Sci 42(7): 1600–1608
8. Matschuk M, Larsen NB (2013) Injection molding of high aspect ratio sub-100 nm nanostructures. J Micromech Microeng 23: 025003
9. Menotti S, Hansen HN, Bissacco G, Calaon M, Tang PT, Ravin C (2014) Injection molding of nanopatterned surfaces in the sub-micrometer range with induction heating aid. Int J Adv Manuf Technol 74(5–8):907–916
10. Lin HY, Chang CH, Young WB (2010) Experimental and analytical study on filling of nano structures in micro injection molding. Int Commun Heat Mass Transfer 37(10):1477–1486
11. Stormonth-Darling JM, Pedersen RH, How C, Gadegaard N (2014) Injection moulding of ultra high aspect ratio nanostructures using coated polymer tooling. J Micromech Microeng 24:075019
12. Lin HY, Young WB (2009) Analysis of the filling capability to the microstructures in micro-injection molding. Appl Math Model 33(9):3746–3755
13. Barbero DR, Saifullah MSM, Hoffmann P, Mathieu HJ, Anderson D, Jones GAC, Welland ME, Steiner U (2007) High-resolution nanoimprinting with a robust and reusable polymer mold. Adv Funct Mater 17(14):2419–2425
14. Stormonth-Darling JM, Gadegaard N (2012) Injection moulding difficult nanopatterns with hybrid polymer inlays. Macromol Mater Eng 297(11):1075–1080
15. Keil M, Beck M, Frennesson G, Theander E, Bolmsjo E, Montelius L, Heidari B (2004) Process development and characterization of antisticking layers on nickel-based stamps designed for nanoimprint lithography. J Vac Sci Technol B 22(6):3283–3287